Boletim da Sociedade Astronômica Brasileira, **37**, no. 1, 22-26

Evolution and final fate of a 9 $M_\odot$ $Z = 0.02$ star

A. Antonini[1] & A. Romero[2]

[1] Universidade Fereral do Rio Grande do Sul e-mail: anacarolina.srantonini@gmail.com, alejandra.romero@ufrgs.br

Abstract. In this work, we study the evolution and final fate of a star with $M_i = 9M_\odot$ and metallicity $Z = 0.02$, using the MESA code. We calculate its entire evolution from pre-Main Sequence to the White Dwarf Cooling Curve, including both the evolution in the TP-SAGB, which we follow for over 100 thermal pulses, and the post-AGB stage. The result is an ultramassive H-deficient WD with an Oxygen-Neon core, surrounded by a thin ^{12}C layer of 5×10^{-3}M$_\odot$ and an He envelope. During the WD stage, we calculate models both with and without phase separation, finding it to produce only a small cooling delay, of 16 Myr . In addition, we examine the effects of fully suppressing the thermal pulsing stage by adopting very high mass-loss rates after the second dredge-up, finding only minor changes to the final mass and composition of the remnant. This is, to our knowledge, the first ultramassive white dwarf sequence for which both the TP-SAGB and post-AGB stages are calculated.

Resumo. Neste trabalho, estudamos a evolução e destino final de uma estrela com M$_\mathrm{i}$ = 9M$_\odot$ e metalicidade $Z = 0.02$, utilizando o código MESA. Calculamos a evolução completa, desde a pré-sequência principal até a curva de resfriamento das anãs brancas, incluindo ambas as etapas de TP-SAGB, a qual seguimos por mais de 100 pulsos, e pós-AGB. O resultado é uma anã branca ultramassiva ausente em hidrogênio, com núcleo de oxígênio-neônio, cercado por uma fina camada de ^{12}C com 5×10^{-3}M$_\odot$ e um envelope de He. Na etapa de Anã Branca calculamos modelos com e sem separação de fases, verificando que ela produz apenas um pequeno atraso, de 16 Myr, no tempo de resfriamento. Além disso, examinamos os efeitos de suprimir completamente a etapa de pulsos térmicos, adotando altas taxas de perda de massa após o segundo dredge-up, encontrando apenas pequenas mudanças na massa e composição final do remanescente. Esta é, dentro da extensão de nosso conhecimento, a primeira sequência de modelos de Anã Branca ultramassiva para qual a evolução em ambas as etapas de TP-SAGB e pós-AGB foram calculadas.

Keywords. star: evolution –(Stars:) white dwarfs – Methods: numerical

1. Introduction

White dwarf (WD) stars are the final stage in the evolution of low- and intermediate-mass stars, which account for more than 95% of the stars in the Galaxy. Although the highest possible mass for a white dwarf star (WD) is a well-established limit (M$_\mathrm{Ch}$ = 1.4 M$_\odot$), the progenitor mass for such a white dwarf is a much more contentious subject.

Different theoretical works find it to occur at different initial masses, which range between ∼7 and 12 M$_\odot$ (Siess 2010; Doherty et al. 2015; Lauffer et al. 2018). This is not merely an effect of metallicity, but rather seems to be the result of calculations adopting different physical prescriptions and parameters for phenomena that lack strong observational constraints. For example, differences in the treatment of convective core boundaries alone can create a spread of over 2M$_\odot$ in the initial mass required for a star to undergo degenerate carbon-burning (Eldridge& Tout 2004; Siess 2010; Farmer, Fields & Timmes 2015). The treatment of mass-loss is another somewhat critical point where models become plagued with uncertainties, especially during the Super-AGB (SAGB) stage. The mechanism responsible for driving stellar winds in this phase is still unclear(Poelarends et al. 2008; Beasor et al. 2020; Cheng et al. 2024), and observational constraints vary by over three orders of magnitude (van Loon et al. 1999; Höfner & Olofsson 2018; Matthews 2024).

Another aspect that encumbers establishing a more accurate maximum mass limit for ultramassive white dwarf (UMWD) progenitors is their very evolution as SAGB stars. After undergoing degenerate carbon burning in the early-AGB, they are expected to experience several tens to hundreds of thermal pulses. The temporal and spatial resolutions required to solve the thermal pulses, combined with the instabilities that arise at the end of this stage and cause computations to stall, make it a computationally challenging and expensive phase. Consequently, very few works have been dedicated to modeling the full evolution of ultramassive WDs, and no models exist in the literature that account for their evolution both in the TP-SAGB and post-AGB stages. And yet, establishing an accurate initial-final mass relation and more fully understanding the characteristics of UMWDs remains imperative if we aim to better constrain the chemical evolution of the Galaxy, the rates for core-collapse supernovae events, and the very nature of type Ia supernovae.

In the past, three different approaches have been taken to create UMWD models. The first considers a polytropic model at the top of the cooling curve as the initial model, where the inner structure of the core, mainly the chemical composition, is taken from a SAGB model before its envelope is stripped (e.g. Córsico et al. 2004; Camisassa et al. 2019; Althaus et al. 2021). The second also starts with a polytropic model at high effective temperatures, but it assumes that the composition is not mass-dependent and either rescales existing WD models to higher masses or creates new UMWD models with a fixed composition (e.g. Benvenuto & Althaus 1999; Schwab 2021; Althaus et al. 2022). The third approach involves fully bypassing the thermal pulses by adopting extreme mass-loss rates in the early AGB phase(e.g. Lauffer et al. 2018).

In this work, we propose an intermediate approach. We calculate a significant fraction of the thermal pulses the star is expected to undergo and force an exit from the TP-AGB before instabilities can halt our calculations, thus allowing the model to undergo post-AGB evolution and finally reach the WD cooling curve. This technique has previously been used by De Gerónimo et al. (2018) to investigate the impact of thermal pulses on the properties of DAVs, and is a somewhat common approach to modeling the previous evolution of CO WDs. We employ the MESA code ((Paxton et al. 2011, 2013, 2015, 2018, 2019; Jermyn et al.

2022) for our calculations and choose a 9 $M_\odot$ Z=0.02 sequence that generates a 1.313 $M_\odot$ WD as a case study.

This document is organized as follows. We briefly describe the physics adopted in our calculations in Section 2. Results and comparisons are presented in Section 3. In Section 4, we conclude with our final remarks.

2. Stellar Modeling

We calculate the complete evolution — from pre-ZAMS to the WD cooling track — of a sequence with initial mass of 9 $M_\odot$ and metallicity Z=0.02, using the unidimensional stellar evolution code MESA [Modules for Experiments in Stellar Astrophysics (Paxton et al. 2011, 2013, 2015, 2018, 2019; Jermyn et al. 2022)] in version r24.08.1.

We adopt the nuclear reaction network `mesa45.net`, which contains 45 isotopes and 367 reactions. Abundance fractions are taken from Asplund, Greveese & Sauval (2009), and our reaction rates are mainly from JINA (Cyburt et al. 2010) and NACRE (Angulo et al. 1999), with a small number of rates from CF88 (Caughlan & Fowler 1988). Supplementary tabulated weak rates are from Langanke & Martínez-Pinedo (2000), Oda et al. (1994), and Fuller, Fowler & Newman (1985). The thermal neutrino loss rates are from Itoh, Nishikawa & Kohyama (1996), and the screening prescription is from Chugunov, DeWitt, & Yakovlev (2007).

We adopt the OPLIB opacity tables (Colgan et al. 2016; Farag et al. 2024), complemented by Ferguson et al. (2005) at low temperatures, and also consider Type 2 opacity tables to account for C and O enrichment. Electron conduction opacities are from Blouin et al. (2020) and Cassisi et al. (2007).

2.1. Pre-WD evolution

During the stages preceding the white dwarf cooling curve, the atmosphere boundary is calculated using the gray Eddington t(tau) relation with uniform opacity. We consider Mixing Length Theory (MLT) (Böhm-Vitense 1958) for treating convection, using the Henyey, Vardya &Bodenheimer (1965) formalism, which allows convective efficiency to vary with opacity, with $\alpha_{\rm MLT} = 2$. We account for element diffusion, adopting the coefficients from Stanton & Murillo (2016). Before the TP-SAGB stage, we determine convective regions using the Ledoux criterion, adopting semi-convection with $\alpha_{\rm semi} = 0.05$ and thermohaline mixing, with $\alpha_{\rm th} = 1$. We further extend the formal convective boundaries by adopting exponential overshooting at the top of the H and He cores and shells, with $f = 0.01$ (Herwig 2000), and in addition, adopt the predictive mixing scheme present in MESA (Paxton et al. 2018) to prevent splitting of the core convective region and the occurrence of breathing pulses. Mass loss prior to the AGB stage is treated using the formula from Reimers (1975), with $\eta_R = 0.3$.

2.1.1. Early AGB and Carbon Burning

As bottom overshooting and thermohaline mixing have been found to dilute the carbon flame, giving origin to hybrid ONeC cores (Denissenkov et al. 2013; Farmer, Fields & Timmes 2015), we disable thermohaline mixing and restrict overshooting to occur only at the upper boundaries of H and He burning shells and non-burning convective zones during this stage. Mass loss is treated with the Bloecker (1995) formulation, with $\eta_B = 0.1$ and a maximum allowed mass-loss rate ($\dot{\rm m}_{\rm max}$) of $10^{-6} M_\odot$/yr.

Carbon burning occurs under degenerate conditions for SAGB stars, making this process very sensitive to temporal and spatial resolution (Siess 2006; Farmer, Fields & Timmes 2015). Thus, we apply additional meshing in the CO core and restrict changes in log LZ, logT, and logP to be smaller than 5% between timesteps. We also force a decrease in the timestep if the central abundances of C, O, or Ne change by more than 0.5% between consecutive steps, adopt "gold2" tolerances, and decrease `varcontrol_target` (w_t) and `time_delta_coeff`(δ_t) to 3×10^{-4} and 0.7, respectively.

2.1.2. TP-AGB

During the TP-AGB stage, we use the Schwarzschild criterion for convection. Overshooting is accounted for only at the bottom of the interpulse convective zone, with $f = 0.008$ (**?**), as inclusion of convective envelope overshooting in models that undergo hot third dredge-up (HTDU) can lead to numerical instabilities (Rees, Izzard & Karakas 2023). We follow the recommendations of Rees, Izzard & Karakas (2023) for resolving the HTDU, adopting $w_t = 2 \times 10^{-5}$, `mesh_dlogX_dlogP_extra`=0.8 for ^{4}He, and `delta_lgL_He_limit`=0.01. We increase the overall number of zones and further increase resolution in He-burning and metal-burning zones. We switch to the `eps_grav` form of the energy equation and do not account for element diffusion. Hydrogen recombination instability (HRI) is handled by adopting the Rees & Izzard (2024) subroutine. We maintain the blocker formulation for mass loss with the same η_B, restricting $\dot{m}$ to a maximum of $10^{-3} M_\odot$/yr (van Loon et al. 1999; Höfner & Olofsson 2018).

To bypass the instabilities that plague SAGB computations, most notably Iron peak instability (FeI), at the end of the TP-AGB phase, and allow calculations to continue, we force an exit from the AGB after over 100 pulses have been calculated. To do that, we increase η_B to 10, limiting $\dot{m}_{max}$ to $1 M_\odot$/yr, and, in addition, we adopt the MESA MLT++ treatment for superadiabaticity (Paxton et al. 2013). To avoid fully removing the H envelope, we gradually reduce $\dot{m}_{max}$ to $10^{-5} M_\odot$/yr when the hydrogen envelope mass ($M_{\rm Henv}$) falls below 0.1 $M_\odot$, completely stopping it once $M_{\rm Henv} < 10^{-5} M_\odot$. After this point, any reduction in the H mass is due to burning.

We revert to the Ledoux criterion during the post-AGB phase and consider thermohaline mixing with $\alpha_{\rm th} = 3$, as it helps smooth chemical discontinuities. We account for element diffusion and employ the formulation by Caplan, Bauer & Freeman (2022) for strongly coupled regimes.

2.2. Evolution on the WD cooling track

During WD evolution, we allow a maximum timestep of 1 Myr. Convection is calculated with the ML2 (Bohm & Cassinelli 1971) formalism for MLT, with $\alpha_{\rm MLT} = 0.8$ (Gianninas Bergeron & Ruiz). The convective regions are determined by the Ledoux criterion before crystallization, and by the Schwarzschild criterion from the onset of crystallization on. We further extend the convective boundaries by adopting exponential overshooting at the bottom of the convective shell with f=0.01, and thermohaline with $\alpha_{\rm th} = 10$. Atmosphere boundaries above 40 000 K are calculated according to the gray Eddington t(tau) relation, with variable opacity. Below 40 000 K, we adopt the atmosphere tables for DA and DB white dwarfs provided by MESA (Rohrmann, Althaus & Kepler 2001; Koester, Kepler &Irwin 2020). We account for element diffusion adopting Caplan, Bauer & Freeman

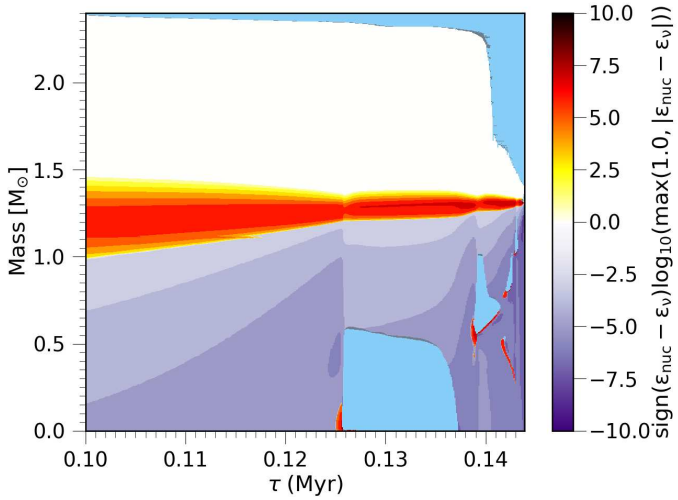

Figure 1. Kippenhahn Diagram following carbon burning in the EAGB. Dark purple regions indicate regions of cooling, primarily from thermal neutrino losses. Red regions indicate significant nuclear burning; light blue regions indicate convection, and grey regions indicate semiconvection. In this plot, time has been reset so that zero is the start of the EAGB.

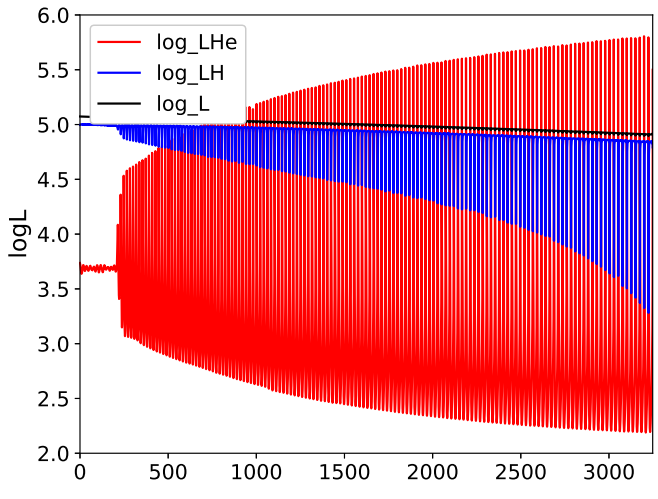

Figure 2. Surface (black), He (red), and H (blue) luminosities as a function of time in the TP-SAGB stage. In this plot, time is reset so that the first He-shell instability corresponds to a time of zero.

(2022) formulation for strongly coupled regimes, and also consider the effects of element sedimentation.

Crystallization is treated self-consistently by Skye (Jermyn et al. 2021), which determines the phase (ϕ) by free energy minimization. Phase separation is calculated using Blouin& Daligaut (2021) phase diagrams for O/Ne mixtures. Our solid mixing rules are from Ogata et al. (1993), and we account for latent heat release and phase separation heating. We do not consider the effects of general relativity or neutrino loss by the Urca process, as their contributions should be negligible or small at our final mass(Schwab 2021; Althaus et al. 2022).

3. Results

We evolve a 9 $M_\odot$, Z=0.02 model starting from the pre-ZAMS until it cools to $\sim$ 10 000 K on the white dwarf cooling track. It results in a $\sim$ 1.313 $M_\odot$ WD, with an ONe core.

3.1. Early-AGB

At the beginning of the EAGB, M_{He} and M_{CO} are 2.328 $M_\odot$ and 1.109 $M_\odot$, respectively, the total stellar mass is 8.91 $M_\odot$ and the model has an age of 31.2 Myr. At this point, the central abundances are X_C=0.33 and X_O=0.63. It is only after $\sim$ 0.12 Myr since the end of CHeB, that Carbon ignites in a flash, when M_{CO} = 1.259 $M_\odot$.

As can be seen in the Kippenhahn diagram of Figure 1, only after the second flash does the efficiency of He-burning significantly decrease, allowing the convective zone to start moving inward. However, before it can fully travel and reach its innermost zone, a semiconvective and later fully convective region is established in the He-burning shell, causing a dredge-out to occur. Similarly to what was found by Doherty et al. (2015), after that the He-shell is extinguished, and the convective envelope penetrates the outward regions of the CO core, slightly reducing M_{CO} by $\sim$ 0.002 $M_\odot$.

At the end of carbon burning, ^{16}O and ^{20}Ne are the most abundant species in the core, corresponding to 47.4% and 39.7%, respectively. This difference is larger in the center, with $X_{^{16}O}$ = 0.514, it decreases at $m_r \sim 0.55 M_\odot$, and finally switches at $m_r \sim 1.0\,M_\odot$, with ^{20}Ne becoming the dominant species in the outer $\sim 0.3 M_\odot$ of the core. Similarly, ^{23}Na is slightly more abundant than ^{24}Mg in the innermost 0.55 $M_\odot$; this switches at this point, and at $m_r \sim 1.0\,M_\odot$, ^{24}Mg becomes significantly more abundant than ^{23}Na, making it our third most abundant species. A similar abundance distribution is also seen in Figure 32 of Iben (Ritossa & García-Berro), for a 1.263 $M_\odot$ core model. However, in that figure, the ^{16}O and ^{20}Ne profiles only approach each other and do not cross.

To verify that we are accurately following the carbon burning stage, we ran additional models where we tested increasing: 1- the spatial resolution,2- the temporal resolution,3- both temporal and spatial resolution. We find very little difference in the global properties and overall evolution of the different tests.

3.2. TP-AGB

We calculate the evolution in the TP-SAGB for 141 pulses, which occur within $\sim$ 3000 yr. During this time, M_{CO} goes from 1.3104 to 1.3126 $M_\odot$, with a remaining envelope mass of 3.91 $M_\odot$.

Figure 2 shows the He, H, and surface luminosities from the first He-shell instability ("mini-pulse") to the last calculated thermal pulse. It takes almost 1000 yr for the helium luminosity to exceed logL, and although the pulses become progressively stronger, L_{He} never reaches $10^{6.0}$ $L_\odot$ during our calculations. This may be a result of truncating the TP-SAGB, but other works that carried out TP calculations also found this feature in their more massive models (Siess 2010; Karakas 2017), so this could be a consequence of their weaker pulses. We also find very inefficient third dredge-ups, with the maximum efficiency $\lambda < 0.02$. Although this may also be an effect of our high mass-loss rate (Rees, Izzard & Karakas 2023), 3DU efficiency varies wildly between works, and there are no observational constraints for it in SAGB stars. Like in all massive SAGB stars, the interpulse period in our model is much shorter than in typical low-mass AGB stars, with an average duration of $\sim$ 20 yr.

We choose to force an exit of the TP-SAGB after the 139th pulse, since from this point onward, the instabilities associated with the end of the TP-SAGB progressively grow, making each consecutive thermal pulse more computationally expensive and

less numerically stable. These instabilities have been extensively discussed in the literature, and we refer the reader to the works of Lau et al. (2012), Doherty et al. (2015), and Rees & Izzard (2024) for in-depth discussions. We have experimented with other strategies to overcome FeI, but find this to be the better suited for the purpose of carrying on calculations in the WD cooling curve.

In addition to running an extra model, where we fully suppress thermal pulses by adopting high winds right after the 2DUP, we also estimate the maximum core growth the star might experience if we were to calculate the thermal pulsing stage to completion. Assuming a constant core growth rate and a mass loss of ($10^{-4}\,M_\odot$/yr), we find that the final mass would be no larger than 1.35 $M_\odot$. From our model without thermal pulses, we find very little difference in the interior mass and composition. Most of the changes in envelope abundances are also small, except for the ^{7}Li content, which is 11 times higher in the sequence that undergoes thermal pulses.

3.3. White Dwarf Evolution

Our calculations result in a white dwarf with a mass of 1.3127 $M_\odot$, a total He mass of $1.5 \times 10^{-5} M_\odot$ and an O/Ne/Mg core. The chemical abundance distribution in our model is such that 47.7% of the total mass is ^{16}O, 39.7% ^{20}Ne, 4.2% ^{24}Mg, 3.3% ^{23}Na, and 0.386% ^{12}C. The remaining $\sim$ 5% are made up mainly of ^{25,26}Mg and ^{27}Al, with only 0.027% being ^{22}Ne. Crystallization starts at an effective temperature of 48 530 K, at a cooling age of only 81Myr.

It takes $\sim$ 160 Myr from the beginning of crystallization to the point where 50% of the star is crystallized, $\sim$ 140 Myr from 50% to 70%, and $\sim$ 270 Myr from 70% to 90%. Phase separation acts along crystallization, modifying the ^{16}O and ^{20}Ne profiles. Figure 3 shows the abundance profiles at four different stages: slightly after the onset of crystallization, when the crystallization front reaches 50% and 70% of the star (in mass), and for our final model. At the time we stop our calculations, when $T_{\rm eff}$ = 9772 K, only the upper $9.4 \times 10^{-4}\,M_\odot$ remains uncrystallized.

We calculate additional models during the WD stage to investigate the effects of phase separation. We find it to introduce a cooling delay of only 16 Myr, and that changing the solid-liquid coexistence regime creates cooling differences that are twice smaller than this.

4. Conclusions

In this work, we have calculated, using MESA r24.08.1, the entire evolution of a 9 $M_\odot$ star with Z=0.02. We detailed its evolution from the EAGB to the WD cooling track, conducting comparisons with alternative models to study the impacts of temporal and spatial resolution, thermal pulse suppression, and phase separation. We report core masses at relevant stages of its evolution and present detailed chemical profiles at the end of the EAGB and TP-AGB, as well as at different temperatures on the WD track.

As a result of our calculations, we find a hydrogen-deficient white dwarf of mass 1.313 $M_\odot$ and He content of $1.5 \times 10^{-5}\,M_\odot$. The interior is 47.7% ^{16}O, 39.7% ^{20}Ne, 4.2% ^{24}Mg, and 3.3% ^{23}Na, making it an O/Ne/Mg WD. The total fractions of ^{12}C and ^{22}Ne are 0.386% and 0.027%, respectively. The inclusion of ONe phase separation introduces a cooling delay of only $\sim$ 16 Myr.

We find that at this mass, the TP-SAGB stage has only a minor effect on the final mass and composition. As such, calculating only the first pulses or altogether skipping thermal pulses, by

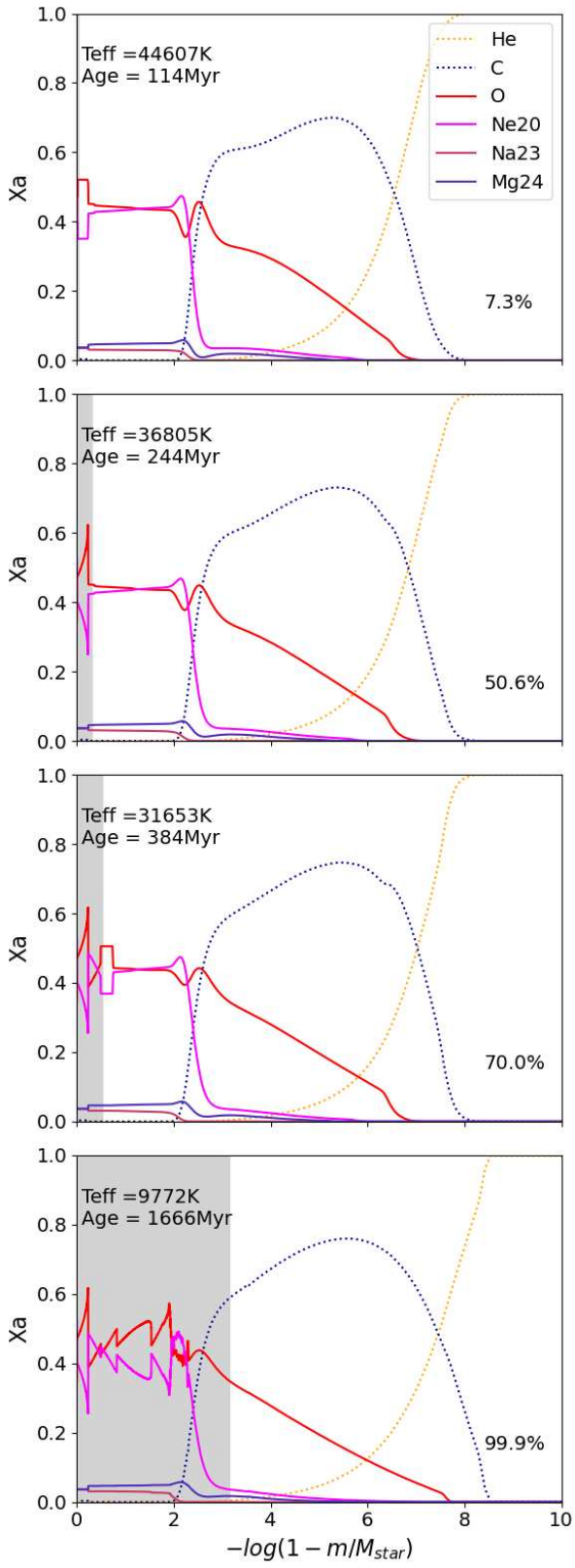

Figure 3. Abundance profiles for our white dwarf sequence with 1.313 $M_\odot$ at four different moments in time. For clarity, we include in the plots only the most relevant species. Panel one shows the abundance profile near the onset of crystallization. Panels 2 and 3 show the profiles when approximately 50% and 70% of the stellar mass is crystallized (gray shaded area), at $T_{\rm eff}$ = 36 800 K and 31 650 K, respectively. We show in the final panel the profile of our last calculated model, at $T_{\rm eff}$ = 9772 K.

adopting a high mass-loss rate **after** the end of the second dredge-up, is a computationally efficient method to create UMWD models from single evolution, with the benefit of reliable chemical compositions.

This is, to our knowledge, the most massive white dwarf model from full evolution for which cooling times and detailed abundance profiles are available in the literature. It is also the only near-Chandrasekhar WD model for which both the TP-SAGB and post-AGB were calculated.

References

Althaus L. G., et al., 2021, A&A, 646, A30
Althaus L. G., Camisassa M. E., Torres S., Battich T., Córsico A. H., Rebassa-Mansergas A., Raddi R., 2022, A&A, 668, A58
Angulo C., et al., 1999, Nuclear Physics A, 656, 3
Asplund M., Grevesse N., Sauval A. J., Scott P., 2009, ARA&A, 47, 481
Bauer E. B., 2023, ApJ, 950, 115
Beasor E. R., Davies B., Smith N., van Loon J. T., Gehrz R. D., Figer D. F., 2020, MNRAS, 492, 5994
Benvenuto O. G., Althaus L. G., 1999, MNRAS, 303, 30
Bloecker T., 1995, A&A, 297, 727
Blouin S., Shaffer N. R., Saumon D., Starrett C. E., 2020, The Astrophysical Journal, 899, 46
Blouin S., Daligault J., 2021, The Astrophysical Journal, 919, 87
Bohm K. H., Cassinelli J., 1971, A&A, 12, 21
Böhm-Vitense E., 1958, Z. Astrophys., 46, 108
Camisassa M. E., et al., 2019, A&A, 625, A87
Caplan M. E., Bauer E. B., Freeman I. F., 2022, MNRAS, 513, L52
Cassisi S., Potekhin A. Y., Pietrinferni A., Catelan M., Salaris M., 2007, The Astrophysical Journal, 661, 1094
Caughlan G. R., Fowler W. A., 1988, Atomic Data and Nuclear Data Tables, 40, 283
Cheng S. J., Goldberg J. A., Cantiello M., Bauer E. B., Renzo M., Conroy C., 2024, The Astrophysical Journal, 974, 270
Chugunov A. I., DeWitt H. E., Yakovlev D. G., 2007, Phys. Rev. D, 76,025028
Colgan J., et al., 2016, ApJ, 817, 116
Córsico A. H., García-Berro E., Althaus L. G., Isern J., 2004, A&A, 427, 923
Cyburt R. H., et al., 2010, ApJS, 189, 240
De Gerónimo F. C., Althaus L. G., Córsico A. H., Romero A. D., Kepler S. O., 2018, A&A, 613, A46
Denissenkov P. A., Herwig F., Truran J. W., Paxton B., 2013, The Astrophysical Journal, 772, 37
Doherty C. L., Gil-Pons P., Siess L., Lattanzio J. C., Lau H. H. B., 2015, MNRAS, 446, 2599
Eldridge J. J., Tout C. A., 2004, MNRAS, 353, 87
Farag E., et al., 2024, ApJ, 968, 56
Farmer R., Fields C. E., Timmes F. X., 2015, ApJ, 807, 184
Ferguson J. W., Alexander D. R., Allard F., Barman T., Bodnarik J. G., Hauschildt P. H., Heffner-Wong A., Tamanai A., 2005, ApJ, 623, 585
Fuller G. M., Fowler W. A., Newman M. J., 1985, ApJ, 293, 1
Gianninas A., Bergeron P., Ruiz M. T., 2011, ApJ, 743, 138
Henyey L., Vardya M. S., Bodenheimer P., 1965, ApJ, 142, 841
Herwig F., 2000, A&A, 360, 952
Herwig F., 2008, Proceedings of the International Astronomical Union, 4, 205–213
Höfner S., Olofsson H., 2018, A&ARv, 26, 1
Iben Jr. I., Ritossa C., García-Berro E., 1997, ApJ, 489, 772
Itoh N., Hayashi H., Nishikawa A., Kohyama Y., 1996, ApJS, 102, 411
Jermyn A. S., Schwab J., Bauer E., Timmes F. X., Potekhin A. Y., 2021, ApJ,913, 72
Jermyn A. S., et al., 2023, ApJS, 265,15
Karakas A. I., 2017, Low- and Intermediate-Mass Stars. Springer International Publishing, Cham, pp 461–481,
Koester D., Kepler S. O., Irwin A. W., 2020, A&A, 635, A103
Langanke K., Martínez-Pinedo G., 2000, Nuclear Phys. A, 673, 481
Lau H. H. B., Gil-Pons P., Doherty C., Lattanzio J., 2012, A&A, 542, A1
Lauffer, G., Romero, A. D., Kepler, S.O.,2018 , MNRAS, 480, 1547
Matthews L. D., 2024, in Hirota T., Imai H., Menten K., Pihlström Y.,eds, IAU Symposium Vol. 380, Cosmic Masers: Proper Motion Toward the Next-Generation Large Projects. pp 275–291
Oda T., Hino M., Muto K., Takahara M., Sato K., 1994, Atomic Data and Nuclear Data Tables, 56, 231
Ogata S., Iyetomi H., Ichimaru S., Van Horn H. M., 1993, Phys. Rev. E, 48, 1344
Paxton B., Bildsten L., Dotter A., Herwig F., Lesaffre P., Timmes F., 2011, ApJS, 192, 3
Paxton B., et al., 2013, ApJS, 208, 4
Paxton B., et al., 2015, ApJS, 220, 15
Paxton B., et al., 2018, ApJS, 234, 34
Paxton B., et al., 2019, ApJS, 243, 10
Poelarends A. J. T., Herwig F., Langer N., Heger A., 2008, The Astrophysical Journal, 675, 614
Rees N. R., Izzard R. G.,Karakas A. I., 2023, Monthly Notices of the Royal Astronomical Society, 527, 9643
Rees N. R., Izzard R. G., 2024, Monthly Notices of the Royal Astronomical Society, 531, 4033
Reimers D., 1975, in , Problems in stellar atmospheres and envelopes, pp. 229–256
Rohrmann R. D., Althaus L. G., Kepler S. O., 2011, MNRAS, 411, 781
Schwab J., 2021, The Astrophysical Journal, 916, 119
Siess L., 2006, A&A, 448, 717
Siess L., 2010, A&A, 512, A10
Stanton L. G., Murillo M. S., 2016, Phys. Rev. E, 93, 043203
van Loon J. T., Groenewegen M. A. T., de Koter A., Trams N. R., Waters L. B. F. M., Zijlstra A. A., Whitelock P. A., Loup C., 1999, A&A, 351,559